Calculation of the angular correlation and the lifetime of positron surface states on metal surfaces

1989 J. Phys.: Condens. Matter 1 2977

(http://iopscience.iop.org/0953-8984/1/18/003)

J. Phys.: Condens. Matter 1 (1989) 2977–2988. Printed in the UK

Calculation of the angular correlation and the lifetime of positron surface states on metal surfaces

Yongming Lou†‡, Binglin Gu§, Jialin Zhu§, Chang Lee§ and Jiajiong Xiong§

† Physics Department, Tsinghua University, Beijing, People's Republic of China
‡ Physics Department, Uppsala University, Box 530, S-75121 Uppsala, Sweden
§ Centre for Theoretical Physics, CCAST (World Laboratory), and Physics Department, Tsinghua University, Beijing, People's Republic of China

Received 20 January 1988, in final form 21 September 1988

Abstract. Using a potential model for the surface of a metal and the revised Brandt–Reinheimer enhancement factor $\Gamma(n)$, we have calculated the electron wavefunction, the two-dimensional angular correlation and the lifetime of 2γ annihilation from the Al(100), Al(110), Al(111) and Cu(121) surfaces. We conclude that (i) the momenta of the electrons are filtered by the surface potential; (ii) the momentum distribution of 2γ annihilation is greatly constricted for both the parallel and perpendicular directions to the surface; (iii) it is possible to obtain simultaneously the observed isotropic angular correlation curve and the long lifetime of the positron surface state; and (iv) within a reasonable range of our model parameters, the isotropy of the angular correlation curve is rather insensitive to the parameter values. Our results are consistent with experiment.

1. Introduction

Over the last decade there has been a spectacular growth in surface science [1]. The loss of periodicity in one direction results in a change in electronic states near and at the surface. In addition, due to the lack of nearest neighbours in one direction there will be a reconstruction of the outer atomic planes at the surface. In general, the surface has the following effects on the electronic structure: (i) the local density of states $N(E, x)$ depends on x near the surface (where E is the energy of the electron and x the axis perpendicular to the surface); (ii) there is some charge redistribution near the surface; and (iii) the surface potential gives rise to an energy-dependent phase shift in the wavefunction and introduces an energy dependence in the normalisation constant. Therefore the momentum distribution of the electrons and the surface electronic properties differ from those in the bulk. Especially near the surface the local Fermi surface is an ellipsoid with the longer axes parallel and the short axis perpendicular to the surface, compared with the spherical Fermi surface in the bulk. Positron annihilation offers a unique way to observe the momentum distribution of electrons in solids [2]. As a result the two-dimensional angular correlation of the 2γ annihilation radiation (2D ACAR) of electron–positrons at the surface is expected to be different from that inside the crystal.

In this paper we propose a potential model to calculate the electron wavefunction. Using the positron wavefunction given by Barton [3], we calculate the two-dimensional angular correlation momentum distribution and the lifetime of positron–electron

0953-8984/89/182977 + 12 $02.50

annihilation from Al(110), Al(100), Al(111) and Cu(121) surfaces. We also adopt a revised Brandt–Reinheimer enhancement factor [4] in an effort to calculate the positron lifetime at these surfaces. Our results agree very well with experimental data.

Lynn and co-workers [5] measured the two-dimensional angular correlation of the 2γ annihilation from a clean Al(100) surface, and discovered that it is substantially distinct from the bulk. Howell *et al* [6] derived similar conclusions from their measurements of 2D ACAR from a copper surface. However, the data can not be explained [5] by the early theoretical work based on either a positron bound in a surface state or a positronium atom weakly bound to the surface [7–11]. A strong anisotropy is predicted in [7–10] which is not in agreement with experiment. Based on the positronium atom model Platzman and co-workers [11] calculated a much narrower shape for the 2D ACAR than that observed.

Most recently, Brown and co-workers [12] also considered the present problem. Their angular correlation curves were obtained using an independent particle model (IPM) and are quite isotropic, but they obtained the perpendicular FWHM larger than the parallel FWHM, contrary to our present results. Since we used a similar IPM model we must identify the differences between their calculations and ours. The reasons for these different results are as follows: Brown and co-workers used a different procedure [13] to calculate the electron wavefunction; from the parametrised form of the electron density without the Friedel oscillations to which the angular correlation curve is quite sensitive, they calculated the electron potential at the surface and then solved the Schrödinger equation numerically to obtain the one-electron wavefunction. Thus an enhancement of high-perpendicular-momentum components of the electron was introduced in [12] by omitting the Friedel oscillation from the parametrised electron density and a different electron potential. Their results using a different approach, namely the mixed density approximation (MDA), show a larger anisotropy than ours. Although the MDA includes electron–positron correlations, it is not suitable for the case of fast spatial variations in the electron density near the surface [14]. The local momentum distribution approximation used in [12] with a local Fermi momentum does not represent correctly the local electronic momentum distribution. This is so since the local electron momentum distribution does not only depend on the local electron density but also depends on the total profile of the electron density, such as the gradient of the density. This is especially important for a surface where there is a fast variation region of density. Besides, in MDA, a somewhat arbitrary cut-off must be used in the calculation of ACAR and the results are quite sensitive to this choice. That is why Brown and co-workers always obtain a substantially larger perpendicular FWHM than parallel FWHM for the ACAR. Based on their calculations Brown and co-workers concluded that their model with reasonable parameters could not give an isotropic momentum distribution. Seeking an alternative explanation for the experimental results, they [15] also calculated the ACAR of a positron localised in a surface monovacancy with the MDA. For this situation one meets the same problems as discussed above. The major question is why the electron annihilating with a positron bound perpendicular to the surface can produce an isotropic angular correlation distribution. In this paper we will provide an answer to this.

There are several methods for calculating the electronic structure of surfaces. Lang [16], using the jellium model, calculated self-consistently the surface electronic structure of simple metals like Na and Al. Although it gives a quite good value for the electronic work function, some local properties, such as the tail of the electron wavefunction, the dipole barrier and the chemical potential are not properly treated in this method. In the transition metals where the d-electrons dominate the bonding, the tight-binding (LCAO)

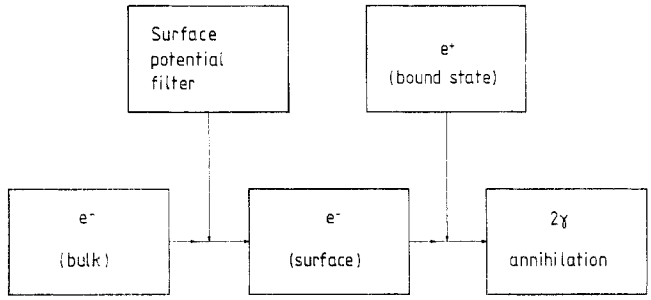

Figure 1. Schematic representation of 2D ACAR coming from the metal surface.

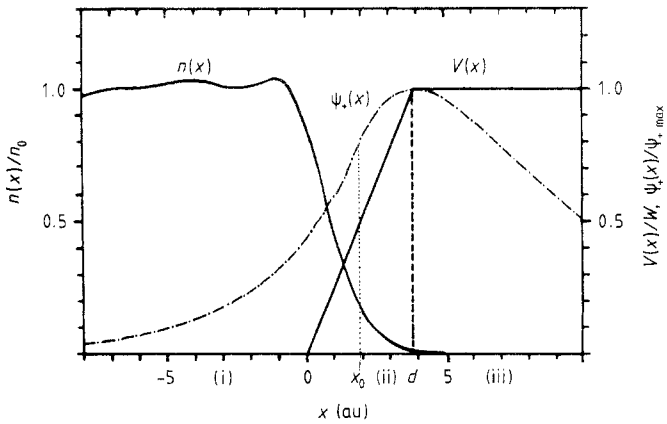

Figure 2. The model electronic potential $V(x)$, the electron density $n(x)$ and positron wavefunction $\psi_+(x)$. W is the Fermi energy E_f plus the work function V_0; n_0 the bulk electron density, $\psi_{+\max}$ the maximum value of $\psi_+(x)$ and x_0 is a parameter of $\psi_+(x)$. Region (ii) is the transitional region of width d.

method provides a useful starting point [17]. The exact surface potential is however very complicated and is still not known very accurately, so instead of using this we use a potential model that can be treated as the parametrised form of the real effective surface potential, to calculate the electron structure of surface. This potential model formalism is especially appropriate for calculating the tail of the wavefunction for electrons near the surface which dominates the electronic as well as other properties. In §§ 2 and 3 we discuss in detail the potential model and the dependence of 2D ACAR distribution on the parameters of the potential model. In the following atomic units are used, i.e., $\hbar = 1$, $m = \frac{1}{2}$, $e^2 = 2$.

2. Theoretical formulation

There are several factors influencing the momentum distribution of the 2γ annihilation of the electron–positron. Figure 1 shows how these factors affect the 2D ACAR. First the surface potential can be treated as a filter similar to an electrical filter. The bulk wavefunctions of electrons are filtered into the surface wavefunctions by the surface potential filter. At this time, both of the higher electronic momenta perpendicular and parallel to the surface are partly reduced by the surface potential, especially for the perpendicular momenta. Then the electron in surface wavefunction annihilates with the positron bound to the surface, and the 2D ACAR comes out.

In discussing theoretically 2D ACAR, the key is to obtain the surface electronic structure, i.e., the tail of the wavefunction for the electrons. We first discuss the solution of the Schrödinger equation. The positive direction of the x-axis is set as perpendicular

to the metal surface. The potential model $V(x, y, z)$ chosen is shown in figure 2 and has the following analytic form:

Table 1. The relevant parameters.

Surface	E_f [18]	V_0	W	d_s	d_a [19]	b [3]	c [3]
Al(100)	0.8551	0.3243 [19]	1.1794	3.827	4.6015	3.75	3.35
Al(110)	0.8551	0.2985 [20]	1.1537	2.706	6.5101	3.7	3.55
Al(111)	0.8551	0.3118 [19]	1.1669	4.418	4.6676	3.65	3.7
Cu(121)	0.5145	0.3329 [21]	0.8474	2.785		4.15[a]	3.2[a]

[a] Because no data are available for Cu(121), we have chosen b and c from Cu(111) data in [3].

$$V(x, y, z) = V(x) \tag{1}$$

where

$$V(x) = \begin{cases} 0 & x \leqslant 0 \quad \text{region (i)} \\ Wx/d & 0 < x < d \quad \text{region (ii)} \\ W & x \geqslant d \quad \text{region (iii).} \end{cases} \tag{2}$$

Here regions (i) and (iii) are the metal and the vacuum, respectively. Region (ii) is the transitional region of width d, which determines the selvedge width and is the only adjustable parameter in the potential model. The parameter d is typically of the order of the planar spacing at the surface. To the authors' knowledge, there are no data available for the selvedge width of the surface. In this paper, therefore, we choose the value of d in three different ways: (i) d is chosen to be equal to the topmost planar spacing at the surface and is represented by d_s: (ii) d is chosen to be the average length of the primitive translation vector of the primitive unit cell on the topmost plane at the surface and is represented by d_a; and (iii) d is used as an adjustable parameter to fit the experimental data. W is equal to the Fermi energy E_f plus the work function V_0, which is surface-dependent. Some relevant parameters are given in table 1.

In this potential model approximation, the three-dimensional Schrödinger equation

$$-\nabla^2\Psi(r) + V(x, y, z)\Psi(r) = E\Psi(r) \tag{3}$$

can be simplified into a one-dimensional equation. In the direction parallel to the surface the electronic wave-function keeps the same form as in the bulk and

$$\Psi(r) = \exp[i(k_y y + k_z z)]\psi(x). \tag{4}$$

Therefore we get the one-dimensional Schrödinger equation

$$-(d^2/dx^2)\psi(x) + V(x)\psi(x) = E_x\psi(x) \tag{5}$$

where

$$E_x = E - k_y^2 - k_z^2. \tag{6}$$

In region (i) we choose $\psi(x) = \psi_1(x)$ and get

$$-(d^2/dx^2)\psi_1(x) = E_x\psi_1(x). \tag{7}$$

Similarly, for regions (ii) and (iii) we have

$$-(d^2/dx^2)\psi_2(x) + (Wx/d)\psi_2(x) = E_x\psi_2(x) \tag{8}$$

$$-(d^2/dx^2)\psi_3(x) + W\psi_3(x) = E_x\psi_3(x). \tag{9}$$

Table 2. The first eleven terms of a_n and b_n.

n	a_n	b_n
0	1	0
1	0	1
2	$-E_x/2$	0
3	$W/6d$	$-E_x/6$
4	$E_x^2/24$	$W/12d$
5	$-WE_x/30d$	$E_x^2/120$
6	$(W^2/d^2 - E_x^3/4)/180$	$-WE_x/120d$
7	$WE_x^2/560d$	$(W^2/d^2 - E_x^3/10)/504$
8	$(-7W^2E_x/6d^2 - E_x^4/24)/1680$	$WE_x^2/3360d$
9	$(W^3/2d^3 - 2WE_x^3/7d)/6480$	$(13W^2E_x/d^2 - E_x^4/4)/9076$
10	$(5W^2E_x^2/d^2 - E_x^5/20)/181440$	$(W^3/d^3 - WE_x^3/4d)/45360$

Solving equations (7–9) we obtain the electron wavefunction as follows

$$\begin{cases} \psi_1(x) = \sin(k_x x + \varphi) \\ \psi_2(x) = \{k_x/[(c_0 k_x)^2 + c_1^2]^{1/2}\}\left(c_0 \sum_{n=0}^{\infty} a_n x^n + c_1 \sum_{n=1}^{\infty} b_n x^n\right) \\ \psi_3(x) = \{k_x/[(c_0 k_x)^2 + c_1^2]^{1/2}\} \exp[-k_x'(x-d)] \end{cases} \tag{10}$$

where

$$k_x = \pm (E_x)^{1/2} \qquad k_x' = (W - E_x)^{1/2}. \tag{11}$$

a_n and b_n are the coefficients of the series solution to equation (8), and obey the following recurrence formulae:

$$\begin{aligned} a_n &= [(W/d)a_{n-3} - E_x a_{n-2}]/[n(n-1)] \\ b_n &= [(W/d)b_{n-3} - E_x b_{n-2}]/[n(n-1)] \end{aligned} \qquad n \geqslant 3 \tag{12}$$

and

$$a_0 = 1 \qquad a_1 = 0 \qquad a_2 = -E_x/2 \qquad b_0 = 0 \qquad b_1 = 1 \qquad b_2 = 0. \tag{12'}$$

Table 2 gives the first eleven terms of a_n and b_n. The phase shift $\varphi(k_x)$ and the coefficients c_0, c_1 are determined by the boundary conditions of the wavefunction at $x = 0$ and $x = d$;

$$\psi_1(0) = \psi_2(0) \qquad \psi_1'(0) = \psi_2'(0) \tag{13}$$

$$\psi_2(d) = \psi_3(d) \qquad \psi_2'(d) = \psi_3'(d) \tag{14}$$

and

$$\begin{aligned} c_0 = &\left(\sum_{n=1}^{\infty} n b_n d^{n-1} + k_x' \sum_{n=1}^{\infty} b_n d^n\right) \\ &\times \left[\left(\sum_{n=0}^{\infty} a_n d^n\right)\left(\sum_{n=1}^{\infty} n b_n d^{n-1}\right) - \left(\sum_{n=1}^{\infty} b_n d^n\right)\left(\sum_{n=1}^{\infty} n a_n d^{n-1}\right)\right]^{-1} \\ c_1 = &\left(-k_x' \sum_{n=0}^{\infty} a_n d^n - \sum_{n=1}^{\infty} n a_n d^{n-1}\right) \\ &\times \left[\left(\sum_{n=0}^{\infty} a_n d^n\right)\left(\sum_{n=1}^{\infty} n b_n d^{n-1}\right) - \left(\sum_{n=1}^{\infty} b_n d^n\right)\left(\sum_{n=1}^{\infty} n a_n d^{n-1}\right)\right]^{-1} \end{aligned} \tag{15}$$

$$\tan \varphi(k_x) = k_x c_0/c_1.$$

Table 3. FWHM for Al(100) with variations in d and x_0. The data labelled d with s represent the value of the topmost planar spacing at the surface. The data labelled a represent the average length of the primitive translation vector of the primitive unit cell on the topmost plane. FWHMx and FWHMy are the FWHM of $I(p_x)$ and $I(p_y)$, respectively. $\Delta\text{FWHM} = \text{FWHM}y - \text{FWHM}x$.

d	3.83^s	3.83^s	3.83^s	3.83^s	3.83^s	3.83^s	3.83^s	7.65	1.91	4.60^a	4.60^a
x_0/d	0	1/16	1/4	1/2	3/4	15/16	1	1/2	1/2	1/2	3/4
FWHMx (mrad)	8.17	8.10	7.89	7.60	7.32	7.15	7.14	6.94	7.92	7.46	7.13
FWHMy (mrad)	8.21	8.14	7.96	7.78	7.69	7.65	7.64	6.36	8.23	7.53	7.40
$\frac{\Delta\text{FWHM}}{\text{FWHM}y}$ (%)	0.5	0.4	0.8	2.4	4.7	6.4	7.1	−9.1	3.8	0.9	3.7

Table 4. FWHM and lifetimes for different surfaces. The data labelled d with s represent the value of the topmost planar spacing at the surface. The data labelled a represent the average length of the primitive translation vector of the primitive unit cell on the topmost plane. FWHMx and FWHMy are the FWHM of $I(p_x)$ and $I(p_y)$, respectively. $\Delta\text{FWHM} = \text{FWHM}y - \text{FWHM}x$.

	Al(100)		Al(110)		Al(111)		Cu(121)
d	3.83^s	4.60^a	2.71^s	6.51^a	4.42^s	4.67^a	2.79^s
x_0/d	1/2	1/2	1/2	1/2	1/2	1/2	0
FWHMx (mrad)	7.60	7.46	7.83	7.17	7.59	7.55	6.53
FWHMy (mrad)	7.79	7.53	8.13	6.86	7.74	7.66	6.32
$\frac{\Delta\text{FWHM}}{\text{FWHM}y}$ (%)	2.4	0.9	3.7	−4.7	1.9	1.4	−3.2
τ(ps)	574	609	551	580	558	556	
Experiment							
FWHMx (mrad)	7.1 ± 0.5 [5]		8.0 ± 0.5 [5]	6.9 [24]			8.0 ± 0.2 [6]
FWHMy (mrad)	7.1 ± 0.5 [5]		8.0 ± 0.5 [5]	6.4 [24]			6.6 ± 0.2 [6]
τ(ps)	580 ± 10 [25]						

The electron density obtained is shown in figure 2 together with the electronic potential model and the positron wavefunction $\psi_+(x)$. The calculated electron density is remarkably close to the self-consistent result of Lang and Kohn [22] and both show Friedel oscillations.

We have recently become aware of work by Sahni and co-workers [23], who have calculated surface dipole barriers, work functions, surface energy, the density of states and the jellium edge by the same model potential as that used in this paper. For metallic densities, the results of the surface dipole barriers, work functions, surface energies and the density of states are also remarkably close to the self-consistent results of Lang and Kohn.

Having obtained the electron wavefunction we now use the positron variational wavefunction given by Barton [3].

$$\psi_+(x) = (2/b)(b+2c)^{-1/2}\{\theta(-x+x_0)a\exp[(x-x_0)/c] + \theta(x-x_0)(x-x_0+a)\exp[(-x+x_0)/b]\} \tag{16}$$

$$a = bc/(b+c)$$

where the parameters b and c depend on both the bulk material and the surface, and are given in table 1. θ is the usual step function, and x_0 is a parameter to fit experimental

Table 5. FWHM for Cu(121) with variations in b, c, d and x_0. FWHMx and FWHMy are the FWHM of $I(p_x)$ and $I(p_y)$, respectively. ΔFWHM = FWHMy − FWHMx.

b	c	d	x_0/d	FWHMx (mrad)	FWHMy (mrad)	$\frac{\Delta\text{FWHM}}{\text{FWHM}y}$ (%)
4.15	3.2	2.79	0	6.53	6.33	−3.2
4.15	3.2	2.79	1/16	6.49	6.30	−3.0
4.15	3.2	2.79	1/2	6.19	6.18	−0.2
4.15	3.2	1.39	0	6.51	6.36	−2.4
4.15	3.2	0.35	0	6.44	6.36	−1.3
4.15	3.2	0.70	0	6.47	6.36	−1.7
4.15	3.2	0.001	0	6.40	6.35	−0.8
2.08	1.6	0.001	0	7.23	5.90	−22.5
1.73	3.2	0.001	0	6.81	6.40	−6.4
1.73	1.33	0.001	0	7.79	5.81	−34.0
1.38	1.07	0.001	0	8.74	5.73	−52.5
Experiment [6]				8.0 ± 0.2	6.6 ± 0.2	−21.2

data and is given in tables 3, 4 and 5. As will be seen below, the result for the angular correlation curve is rather insensitive to the actual value of x_0.

Using the independent particle approximation [26] we have calculated the momentum distribution $\rho^{2\gamma}(\boldsymbol{p})$ of the annihilating positron–electron

$$\rho^{2\gamma}(\boldsymbol{p}) = \text{constant} \times \sum_{i}^{\text{occ}} \left| \int \mathrm{d}\boldsymbol{r} \exp(-\mathrm{i}\,\boldsymbol{p}\cdot\boldsymbol{r})\Psi_+(\boldsymbol{r})\Psi_i(\boldsymbol{r}) \right|^2 \tag{17}$$

where $\boldsymbol{p}$ is the total momentum of 2γ photons. In equation (17), there are two kinds of important common integrations, INT1 (p_x, n) and INT2 (p_x, n), which are related to the transitional region as follows:

$$\begin{aligned}
\text{INT1}(p_x, n) &= \int_0^{x_0} \mathrm{d}x \exp(-\mathrm{i}p_x x) x^n a \exp[(x - x_0)/c] \\
&= a \exp(-\mathrm{i}p_x x_0) \sum_{m=1}^{n+1} (-1)^{m-1} \frac{x_0^{n+1-m}}{(1/c - \mathrm{i}p_x)^m} \frac{n!}{(n+1-m)!} \\
&\quad - (-1)^n a \exp\left(\frac{-x_0}{c}\right) \frac{n!}{(1/c - \mathrm{i}p_x)^{n+1}}
\end{aligned} \tag{18}$$

$$\begin{aligned}
\text{INT2}(p_x, n) &= \int_{x_0}^{d} \mathrm{d}x \exp(-\mathrm{i}p_x x) x^n \exp[(-x + x_0)/b] \\
&= -\exp\left(-\mathrm{i}p_x d - \frac{(d - x_0)}{b}\right) \sum_{m=1}^{n+1} \frac{d^{n+1-m}}{(1/b + \mathrm{i}p_x)^m} \frac{n!}{(n+1-m)!} \\
&\quad + \exp(-\mathrm{i}p_x x_0) \sum_{m=1}^{n+1} \frac{x_0^{n+1-m}}{(1/b + \mathrm{i}p_x)^m} \frac{n!}{(n+1-m)!}
\end{aligned} \tag{19}$$

where $n = 0, 1, 2, 3, \ldots$.

The 2D angular correlation $I(p_x, p_y)$ is

$$I(p_x, p_y) = \int \rho^{2\gamma}(\boldsymbol{p})\, \mathrm{d}p_z \tag{20}$$

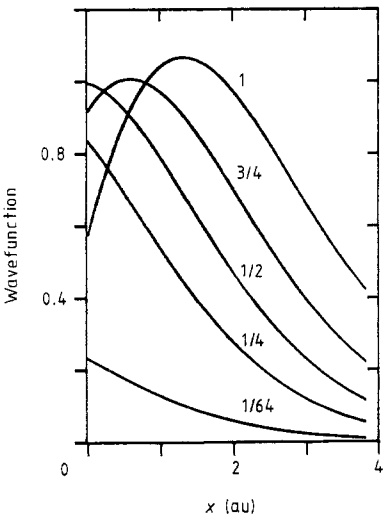

Figure 3. Electron wavefunction $\psi_2(x)$ with different momenta k_x in the transitional region of an Al(100) surface. The labelling of the curves (1, 3/4, 1/2, 1/4 and 1/64) represents their ratios of k_x^2 to k_f^2.

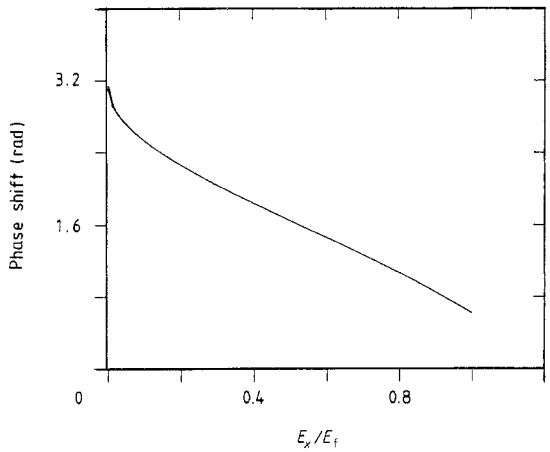

Figure 4. Phase shift $\varphi(E_x)$ of the electron wavefunction near an Al(100) surface.

and the one-dimensional angular correlation $I(p_x)$ and $I(p_y)$ are respectively

$$I(p_x) = \int I(p_x, p_y)\,\mathrm{d}p_y \tag{21}$$

$$I(p_y) = \int I(p_x, p_y)\,\mathrm{d}p_x. \tag{22}$$

The positron lifetime τ and the total annihilation rate λ are calculated with the local density approximation [27].

$$1/\tau = \lambda = \int_{-\infty}^{\infty} \mathrm{d}x\,|\psi_+(x)|^2 \Gamma[n(x)] \tag{23}$$

$$n(x) = (1/\pi^2) \int_0^{k_f} (k_f^2 - k_x^2)|\psi(k_x, x)|^2\,\mathrm{d}k_x \tag{24}$$

where n is the electron density and k_f is the Fermi momentum. For the enhancement form $\Gamma(n)$ we use [4] a revised Brandt–Reinheimer form

$$\Gamma(n) = \{2\theta[r_{sc} - r_s(n)] + 134n\} \times 10^9\ \mathrm{s}^{-1} \tag{25}$$

where the density parameter r_s is equal to $(4\pi n/3)^{-1/3}$ and r_{sc} is a cut-off parameter in the low-density region. When r_{sc} is set equal to infinity, $\Gamma(n)$ in equation (25) becomes the Brandt–Reinheimer form [27]. The Brandt–Reinheimer form gives a poor upper limit of 500 ps for the positron lifetime in vacuum, which is contrary to the experimental positron lifetime at the surface. With this revised form we need only to use a sufficiently large r_{sc} to obtain the correct positron lifetime in the large open-volume defect at the surface and still keep all previous calculations for positron lifetimes in the bulk, vacancies and other small open-volume defects unchanged.

3. Results and discussion

In figure 3 we show the electron wavefunction $\psi_2(x)$ for different values of the momentum k_x in region (ii) of an Al(100) surface. It is easy to see that, for low momentum k_x, $\psi_2(x)$ decays more rapidly than for higher k_x, i.e., only electrons with higher perpendicular momentum have a large probability to pass through the transitional region. At the same time most of the electrons with higher k_x usually have lower parallel momenta because the largest total momentum of the electron cannot be larger than the Fermi momentum. On the one hand, the electronic wavefunction with higher parallel momentum (and consequently lower perpendicular momentum) decays more rapidly than those with a lower parallel momentum. This causes the parallel part of the 2D ACAR to become narrower. On the other hand, unlike the parallel momentum of the electron which is conserved and is a good quantum quantity, the perpendicular momentum of

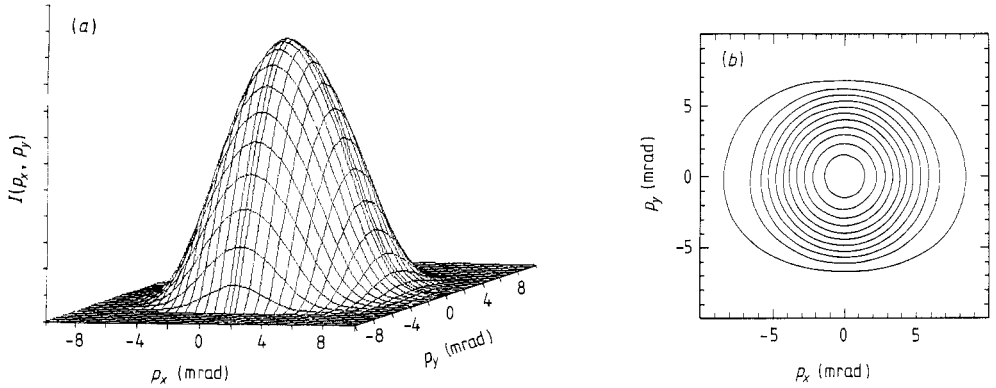

Figure 5. (*a*) Theoretical two-dimensional angular correlation distribution $I(p_x, p_y)$ of 2γ annihilation near an Al(100) surface. $d = 3.827$ au and $x = 1.914$ au. (*b*) Calculated contour plot of $I(p_x, p_y)$ in figure 5(*a*).

the electron is not conserved and is reduced by the surface potential in the transitional region, narrowing the perpendicular part of the 2D ACAR. The majority of the positron–electron annihilation occurs in the region where both the distribution of perpendicular and parallel momenta of the electron is narrower than those in the bulk, and the distribution of the perpendicular momentum of the electron is much narrower than it is for the parallel one. In other words, in this region the momentum distribution of the electrons has a narrower ellipsoid shape with the long axes parallel and the short axis perpendicular to the surface. Therefore in both directions the 2D ACAR will be compressed and its shape will be nearly isotropic in spite of the presence of a positron near the outer surface.

The phase shift $\varphi(E_x)$ of the electron wavefunction for Al(100) is shown in figure 4. At $E_x = 0$, $\varphi(0) = \pi$. In our linear potential model for the surface, $\varphi(E_x)$ has a nearly linear dependence on E_x/E_f. For small values of E_x, $\varphi(E_x) - \pi$ and $\psi_1(0)$ are also small. According to the above discussion, this again means that 2D ACAR is compressed in both directions.

The theoretical 2D ACAR $I(p_x, p_y)$ near the Al(100) surfaces is shown in figure 5(*a*). It is quite isotropic, which is consistent with experiment [5]. Figure 5(*b*) shows contours of the same data as (*a*). In the central part of the contours, the parallel part of $I(p_x, p_y)$ is larger than the perpendicular part, in good agreement with experiment. To the authors' knowledge, no previous calculations have provided this result, but have given that the

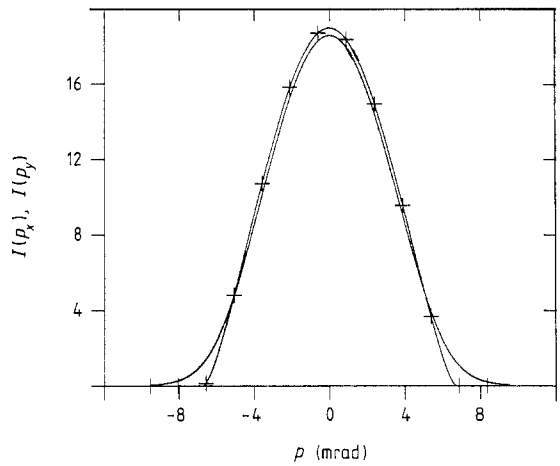

Figure 6. One-dimensional angular correlation $I(p_y)$ for momentum parallel to Al(100) surface and $I(p_x)$ for momentum perpendicular to the surface. The curve through the crosses represents $I(p_y)$.

perpendicular part of the $I(p_x, p_y)$ is always larger than the parallel part. In the outer part of the (p_x, p_y) plane we find that the perpendicular part of $I(p_x, p_y)$ is larger than the parallel part, again in agreement with experiment. To show the shape of $I(p_x, p_y)$ more clearly, we present the 1D ACAR momentum distribution along p_x and p_y in figure 6. In table 3, we give the FWHM of the 1D ACAR along the perpendicular direction FWHMx and along the parallel direction FWHMy for the Al(100) surface for different choices of d and x_0. It is easily seen that: (i) for most of the values of d and x_0 listed in table 3, FWHMy is larger than FWHMx, except when $d = 7.6540$ and $x_0 = d/2$. (ii) For reasonable values of d and x_0, the isotropy of $I(p_x, p_y)$ is not very sensitive to x_0. (iii) When d is chosen to be equal to d_a, the average length of the primitive translation vector of the primitive unit cell on the topmost plane at the surface, both results (FWHMx = 7.4606 mrad and FWHMy = 7.5341 mrad when $x_0/d = \frac{1}{2}$, and FWHMx = 7.1368 mrad and FWHMy = 7.4026 mrad when $x_0/d = \frac{3}{4}$) are completely consistent with the experimental value 7.1 ± 0.5 mrad [5] for both directions in the Al(100) surface. In processing the experimental data in [5, 28], the p_y (parallel) = 0 point was chosen to minimise the antisymmetric component of the data, and varying the p_x (perpendicular) = 0 position by ±0.15 mrad leads to at most a 10% anisotropy with the parallel component being larger. The experimental FWHM has a slightly different value than in [5], if a different method of data processing is used. Our results are therefore in good agreement with experiment.

We show the FWHM for the different surfaces in table 4. For Al(110) there are two different experimental values. In [5], both FWHMs are 8.0 ± 0.5 mrad. In [24] FWHMx = 6.9 mrad and FWHMy = 6.4 mrad. If we choose $d = d_s$, the calculated values are in agreement with the data in [5]. If $d = d_a$, the calculated values are consistent with the data in [24]. For the choice of d we need more information to decide which one is to be preferred. For Al(100) and Al(111), both choices of d give similar results.

For the Cu(121) surface, we have not found the positron parameters b and c, so we use b and c from the data of the Cu(111) surface in [3] or take them as adjustable parameters. In table 5, we list the FWHM as a function of b and c. The experimental data for Cu(121) is substantially different from the value for Al. The theoretical FWHM in the bulk of Cu is 7.40 mrad for one valence electron per atom, while for Cu(121) surface the experimental FWHMx = 8.0 ± 0.2 mrad [6] and FWHMy = 6.6 ± 0.2 mrad. The experimental FWHM in the bulk of Cu is 10.2 mrad [29]. In this case the contribution of the d electron must be taken into account. Further work on this problem is currently in progress and will be discussed elsewhere.

In table 4 we also show the positron lifetime calculated for the three surfaces of Al with $r_{sc} = 20$ in equation (25). It is easy to see that this choice corresponds to a density of $n(r_{sc}) = 0.298 \times 10^{-4}$, which is 0.11% of the bulk density. The theoretical lifetime is now in very good agreement with the experimental result. At the same time this choice does not change all previous calculations for positron lifetimes in bulk and in small open-volume defects because of the very low cut-off for the electron density. A more realistic enhancement factor $\Gamma(n)$ would be one where $\Gamma(n)$ behaves smoothly rather than discontinuously.

In our potential model formalism, the linear potential $V(x)$ in region (ii) (see equation (2)) can be replaced by a polynomial to account for a different surface of a different metal. Besides the shape of $V(x)$, the width d and the work function V_0 are the most important factors which affect the shape of the 2D ACAR. For the different surfaces of the same metal or for a different metal, V_0 and d will be changed. Therefore the shape of the 2D ACAR for different surfaces will be different. The larger the values of V_0 and d, the narrower is the shape of the 2D ACAR.

More recently, Rubaszek and co-workers [30] claimed that the strong electron–positron correlations are responsible for the isotropic experimental result, but the enhancement factors used in their paper are obtained from the bulk electron and bulk positron states, which are not suitable to deal with the surface problem and result in a much narrower shape of the 2D ACAR distribution than the experimental one. We believe that the exact electron–positron correlation enhancement does not change the isotropic result appreciably for the simple metal surface.

In summary, we have shown that our potential model can give a correct description that electrons with different momenta are filtered by the surface potential. Near the surface the local Fermi surface is an ellipsoid with the longer axes parallel and the short axis perpendicular to the surface. In this formalism the 2D ACAR for both directions should be compressed; in some cases its shape is almost isotropic, while in others it may be anisotropic. For different metals and different surfaces the constriction of the 2D ACAR are different. In the present work we have shown that it is possible to obtain simultaneously the observed isotropic angular correlation curve and the long lifetime of the positron surface state. For a reasonable range of the parameters in our model, the near isotropy of the angular correlation curve is rather insensitive to the value of x_0.

Acknowledgments

The authors wish to acknowledge stimulating discussions with Professor S Berko and helpful discussions with Professor He Yuanjin. We would also like to thank Professors B Johansson, R Nieminen and R N West for their comments on the manuscript. The help of Dr Chen Daton in plotting is also gratefully acknowledged.

References

[1] Prutton M 1983 *Surface Physics* ed. M Prutton (Oxford: Clarendon) p 3
[2] Howell R H, Alvarez R A, Woodle K A, Dhawan S, Egan P O, Hughes V W and Ritter M W 1983 *IEEE Trans. Nucl. Sci.* **NS–30** 1438
[3] Barton G 1982 *J. Phys. C: Solid State Phys.* **15** 4727
[4] Lou Yongming, Gu Binglin, Zhu Jialin, Lee Chang and Xiong Jiajiong 1988 *Phys. Rev.* B **38** 9490
[5] Lynn K G, Mills A P Jr, West R N, Berko S, Canter K F and Roellig L O 1985 *Phys. Rev. Lett.* **54** 1703
[6] Howell R H, Meyer P, Rosenberg I J and Fluss M J 1985 *Phys. Rev. Lett.* **54** 1698

[7] Hodges C H and Stott M J 1973 *Solid State Commun.* **12** 1153
[8] Nieminen R and Manninen M 1973 *Solid State Commun.* **15** 403
[9] Rozenfeld B *et al* 1983 *Acta Phys. Pol.* A **64** 93
[10] Garner J and Benedek R 1986 *J. Phys. F: Met. Phys.* **16** L165
[11] Platzman P M and Tzoar N 1986 *Phys. Rev.* B **33** 5900
[12] Brown A P, Walker A B and West R N 1987 *J. Phys. F: Met. Phys.* **17** 2491
[13] Brown A P private communication
[14] Arponen J, Hautojärvi P, Nieminen R and Pajanne E 1973 *J. Phys. F: Met. Phys.* **3** 2092
[15] Brown A P, Jensen K O and Walker A B 1988 *J. Phys. F: Met. Phys.* **18** L141
[16] Lang N D 1973 *Solid State Phys.* **28** 225 (New York: Academic)
[17] Friedel J 1973 *J. Phys. F: Met. Phys.* **3** 785
[18] Kittel C 1976 *Introduction to Solid State Physics* ed. C Kittel (New York: Wiley) p 155
[19] Grepstad J K, Gartland P O and Slagsvold B J 1976 *Surf. Sci.* **57** 348
[20] Eastment R M and Mee C H B 1973 *J. Phys. F: Met. Phys.* **3** 1738
[21] Gartland P O 1972 *Phys. Norv.* **6** (3, 4) 201
[22] Lang N D and Kohn W 1970 *Phys. Rev.* B **1** 4555
[23] Sahni V, Ma C Q and Flamholz J S 1978 *Phys. Rev.* B **18** 3931
[24] Chen D M, Berko S, Canter K F, Lynn K G, Mills A P Jr, Roellig L O, Sferlazzo P, Weinert M and West R N 1989 unpublished
[25] Lynn K G, Frieze W E and Schultz P J 1984 *Phys. Rev. Lett.* **52** 137
[26] Berko S 1983 *Positron Solid State Physics* ed. W Brandt and A Dupasquier (New York: North-Holland) p 64
[27] Brandt W and Reinheimer J 1971 *Phys. Lett.* **35A** 109
[28] Chen D M, Berko S, Canter K F, Lynn K G, Mills A P Jr, Roellig L O, Sferlazzo P, Weinert M and West R N 1987 *Phys. Rev. Lett.* **58** 921
[29] Berko S and Plaskett J S 1958 *Phys. Rev.* **112** 1877
[30] Rubaszek A, Lach J, Brown A and Walker A 1988 *Proc. 8th Int. Conf. Positron Annihilation (Gent, Belgium) 1988*